arXiv:1607.04652v1 [cond-mat.dis-nn] 8 Jul 2016

Many-Body Localization in System with a Completely Delocalized Single-Particle Spectrum

Yevgeny Bar Lev,[1,*] David R. Reichman,[1] and Yoav Sagi[2]

[1] *Department of Chemistry, Columbia University, 3000 Broadway, New York, New York 10027, USA*

[2] *Department of Physics, Technion – Israel Institute of Technology, Haifa 32000, Israel*

Many-body localization (MBL) in a one-dimensional Fermi Hubbard model with random on-site interactions is studied. While for this model all single-particle states are trivially delocalized, it is shown that for sufficiently strong disordered interactions the model is many-body localized. It is therefore argued that MBL does not necessary rely on localization of the single-particle spectrum. This model provides a convenient platform to study pure MBL phenomenology, since Anderson localization in this model does not exist. By examining various forms of the interaction term a dramatic effect of symmetries on charge transport is demonstrated. A possible realization in a cold atom experiments is proposed.

PACS numbers: 71.23.An, 72.15.Rn, 05.60.Gg

Introduction.–It has been known for almost 60 years that *non-interacting* particles in one-dimensional disordered systems exhibit Anderson localization [1]. Transport in these systems is exponentially suppressed with the system size, and without coupling to the environment, these systems are non-ergodic at any temperature. Anderson localized systems are, however, non-generic, since they do not include interactions which allow for the exchange of energy. For many years it was assumed that interactions generally restore ergodicity and destroy localization [2]. A decade ago, using non-equilibrium diagrammatic techniques, it was argued that Anderson localization is stable under the addition of a small short-ranged interactions [3], a phenomenon currently known as many-body localization (MBL). Many-body localized systems are the only known *generic* non-ergodic systems which do not follow the assumptions of statistical mechanics [4–6]. While the realization of MBL systems presents challenges in condensed matter systems due to inevitable presence of phonons [7, 8], recent experiments in cold atoms have provided evidence of the existence of MBL in both one-dimensional [9–11] and two-dimensional systems [12].

To establish the existence of MBL, the seminal work of Basko, Aleiner and Altshuler assumes the presence of quenched disorder and localization of *all* single-particle states [3]. It is currently under debate whether quenched disorder is necessary for the existence of MBL. A number of numerical studies of *translationally invariant* systems with no quenched disorder have been carried out. However, due to large finite size effects these studies are inconclusive with respect to localization [13–20]. A related question, whether MBL can exist in a system where only *some* of the single-particle states are delocalized, namely in systems with a mobility edge in the single-particle spectrum, has been affirmatively answered [21–24]. In our work, we go one step beyond, and completely abolish the assumption of localization of single-particle states. We show that many-body localization is possible when the non-interacting limit is trivial, namely when *all* single-particle states are completely delocalized. A related result has been discussed from a different perspective in a recent study of the XXZ model (see Appendix of Ref. [25]). While previously studied MBL systems could be viewed as continuous deformations of the Anderson insulator [26, 27], much in the same vein as a Fermi liquid is a continuous deformation of a Fermi gas, our work suggests that there are distinct classes of systems exhibiting MBL that differ in their global symmetries.

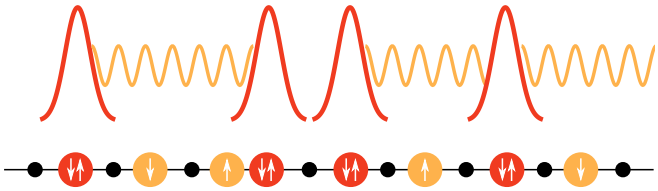

Figure 1. A schematic of the model considered in this work. The lower portion of the figure shows a random configuration of particles. The red (dark) particles are doublons, and the orange (light) particles are singlons. The upper portion of the figure is a cartoon of the charge distribution, with localized doublons and delocalized singlons.

Model.–We study the dynamical properties of one-dimensional Fermi Hubbard model with a random interaction term,

$$\hat{H}_{ns} = -t_h \sum_{\sigma,i=1}^{L-1} \left(\hat{c}^{\dagger}_{i\sigma} \hat{c}_{i+1,\sigma} + \hat{c}^{\dagger}_{i+1,\sigma} \hat{c}_{i,\sigma} \right) + \sum_{i=1}^{L} U_i \hat{n}_{\uparrow i} \hat{n}_{\downarrow i}, \tag{1}$$

where L is the length of the lattice, $\hat{c}^{\dagger}_{i\sigma}$ ($\hat{c}_{i\sigma}$) is the creation (annihilation) operator of site i and spin σ obeying the usual anti-commutation relations, $\hat{n}_{i\sigma} = \hat{c}^{\dagger}_{i\sigma} \hat{c}_{i\sigma}$ is the number operator, t_h is the hopping strength, which we will set to one, the interaction terms U_i are random and uniformly distributed on the interval $-\Delta U \leq U_i \leq 0$. We

use a definite (attractive) sign of the interaction, but for the infinite temperature limit considered here, we have verified that the sign of the interaction does not change the conclusions of our work. The single particle states of this model are simple plane waves and therefore without interactions this model is trivially delocalized and thus cannot be studied by the perturbation theory developed in Ref. [3]. It also cannot be studied by the local unitary diagonalization technique of Ref. [27], since the starting diagonal Hamiltonian is highly degenerate. Nevertheless, some intuition can be acquired by considering the hopping term as a perturbation. At the lowest non-trivial order in the hopping, the model effectively contains two species (see Fig. 1): doubly charge excitations - doublons, and singly charge excitations - singlons. The singlons are light and hop at a rate, t_h, while the doublons are heavy and hop at the average rate $\sim 4t_h^2/\Delta U$. Since the interaction is random, the doublons are strongly localized, while, the singlons do not see an effective disordered potential, and thus are delocalized. Nevertheless, for any initial state with a finite doublon density, the doublons serve as "random barriers" to the singlons, which leads to their localization.

Results.–To verify that over time the singlons do not delocalize the doublons we use numerically exact methods: exact diagonalization (ED) and time-dependent density matrix renormalization group (tDMRG) [28]. We calculate the spread of a charge excitation at infinite temperature, by evaluating the correlation function,

$$C_i(t) = \frac{1}{\mathrm{Tr}\ \hat{P}} \mathrm{Tr}\ \hat{P}\left(\hat{n}_i(t) - 1\right)\left(\hat{n}_0 - 1\right), \qquad (2)$$

where $\hat{P}$ is a projector, which we define as $\hat{P}_s$ (no doublons), $\hat{P}_d$ (no singlons) and $\hat{I}$ (infinite temperature), and $\hat{n}_i \equiv \hat{n}_{i\uparrow} + \hat{n}_{i\downarrow}$, measures the total charge (or total number of atoms, in the case of neutral ultracold atoms) at site i. Since we aim to demonstrate localization, we fix the disordered interaction to be large enough (see Ref. [29]), $\Delta U = 30$, and leave the exploration of transport *across* the MBL transition for a subsequent work. To characterize the spread of the charge excitation we calculate its width as a function of time,

$$\sigma^2(t) = \sum_i i^2 C_i(t), \qquad (3)$$

and average it over random initial configurations of the particles as well as the disordered interaction. To eliminate finite size effects, we make sure that the excitation has not reached the boundaries of the system for the simulation times, which is achieved by correspondingly increasing the size of the system. Thus the dynamics we calculate correspond to the bulk limit up to all times observed. In Fig. 2 we present results of tDMRG simulations for a system of size $L = 20$ at an average filling of 0.5. For this simulation we have used a discarded weight

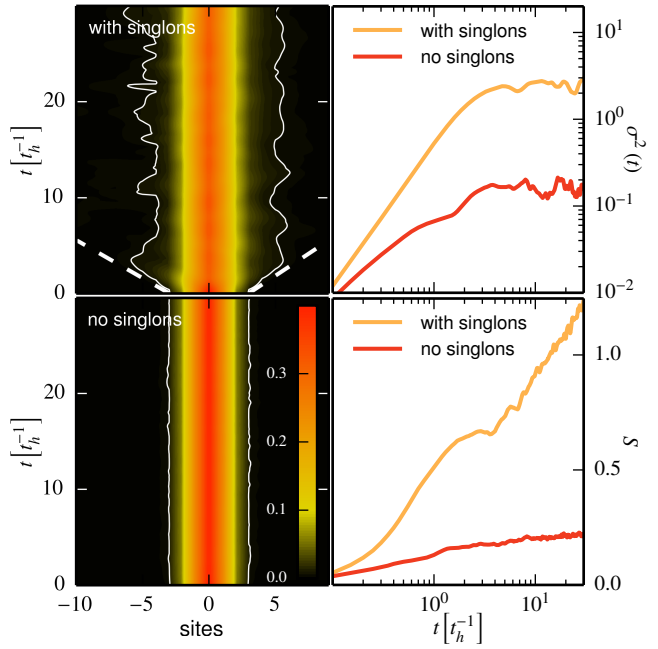

Figure 2. Charge excitation dynamics of the random interaction Fermi-Hubbard model (1) with and without singlons in the initial state. The left panels display contour plots of the correlation function, $C_i(t)$, as a function of space and time. The solid white line corresponds to the contour line, $C_i(t) = 7.5 \times 10^{-3}$, and the dashed white lines highlight ballistic jets of singlons. The top right panel presents the width of the excitation as a function of time on a log-log plot, and the bottom right panel the entanglement entropy S as a function of time on a semi-log plot. The data has been obtained using tDMRG for $L = 20$ and $\Delta U = 30$, and averaged over a minimum of 300 realizations.

of $\chi = 10^{-9}$, a second order Trotter decomposition, and a step size of $\delta t = 0.05$. We have ensured that within statistical error the result is converged with respect to the time step and the discarded weight. On the left side of Fig. 2 we compare the spread of charge excitation starting from two different initial conditions. On the bottom panel we exclude singlons $\left(\hat{P} = \hat{P}_d\right)$ from the initial random configurations of charges, while on the top panel singlons are not excluded $\left(\hat{P} = \hat{I}\right)$. With singlons the excitation has initial ballistic jets which disappear on length scales longer than the mean free path of the singlons, which for infinite temperatures considered here, corresponds to the average distance between the blocking doublons ($l_e \approx 4$). As can be seen from the bottom left panel, the ballistic jets vanish after singlons are removed from the initial configurations. For both initial conditions, the width of the excitation of the charge initially grows ballistically, but then saturates to a finite plateau value, indicating localization (right top panel). The entanglement entropy growths logarithmically, which is typical for many-body localized systems [30, 31]. For random initial charge con-

figurations *without* doublons the excitation appears delocalized for timescales on which bulk transport is accessible (data not shown). While the putative delocalization of this initial condition could be a result of a mobility edge, the strength of the disordered interaction was chosen such that *all* many-body states are localized, namely there is *no* mobility edge (see Supp. Matt. [29]). After a short time (see next paragraph) a finite density of doublons of the order of $O(1/U)$ will be generated, which will result in eventual localization of the singlons. The expected localization length should be at least of the order of the distance between the doublons, $\lambda_s \approx U = 30$, and is beyond the system sizes and times available in our simulations. The dramatic difference in short time dynamics, highlights the importance of proper selection of initial conditions for cold atom experiments. While the system is localized for a *typical* initial condition (as we see from Fig. 2), the initial configurations without doublons can show putative delocalization for quite long times. Although these states are of measure zero in the thermodynamic limit, they are still realizable in cold atom experiments, where the density of doublons or singlons can be effectively controlled [9].

There are three different simple time-scales in model (1): $t_s = t_h^{-1}$, which corresponds to hopping of the singlons, $t_d \sim U/\left(4t_h^2\right)$, which corresponds to hopping of the doublons and for temperatures, $T \ll U$, there is a time scale which corresponds to the decay (generation) of the doublons. This timescale can be formidably long, $t_{\text{decay}} \sim \exp(cU)$ (where c is some constant) [32, 33], however, for infinite temperatures studied here, thermal fluctuations provide the necessary energy to break the doublon apart, such that doublons decay occurs at the timescale of t_s. Therefore the longest time-scale in our problem is t_d. To verify that the observed localization exists also for times much larger than this timescale namely, $t \gg t_d \approx 7$, we utilize exact diagonalization. As is clear from Fig. 2, without the singlons the excitation is effectively contained in a region of less than 10 sites. We therefore limit our exact diagonalization simulations to system sizes $L = 7$ and $L = 9$. In Fig. 3 we show the width of the excitation as a function of time up to time $t = 100$, starting from an initial state without singlons. Clearly, localization persists up to this time, and finite size effects are negligible. This can be also inferred from the profile of the excitation at the final time of the simulation, which lies away from the boundaries (see left panel). We can also compare to the dynamics in the *clean* case, with same interaction strength, $U_i = -30$. In this case, the model can be effectively described by the Heisenberg model [34]. Over the same timescale for which localization persists in the *disordered* system, in the *clean* system the excitation rapidly spreads over the entire lattice (see left panel). The entanglement entropy spreads ballistically (not shown), and bulk charge transport (before the excitation has reached the boundaries)

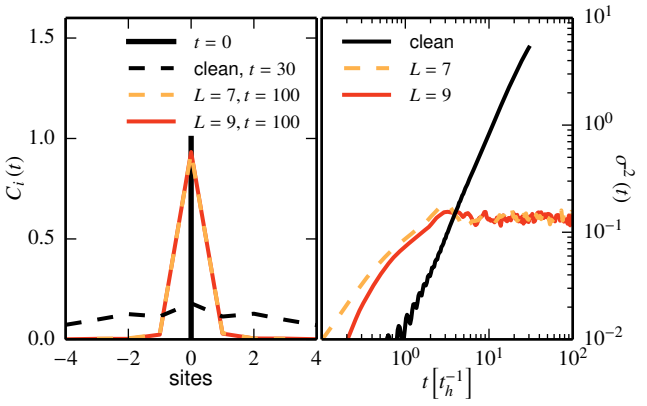

Figure 3. Charge excitation dynamics for clean and disordered Hubbard models starting from a random charge configuration without singlons. *Right panel*: charge excitation width as a function of time for disordered colored (gray) lines and clean Hubbard models (black dashed line) on a log-log plot. The parameters used for the disordered case are $-30 \leq U_i \leq 0$, and for the clean case $U_i = -30$. *Left panel*: Excitation profile for the initial (full black line) and final times (gray, and dashed black lines).

is super-diffusive, $\sigma^2(t) \propto t^{1.65}$, consistent with previous studies [35][36]. We therefore conclude that the observed localization is *not* related to the slow drift of the doublons over timescale, t_d, but is true many-body localization.

After establishing localization for the model (1) we consider the effect of symmetries on non-equilibrium dynamics. We add an additional $SU(2)$ symmetry in the charge sector by changing the interaction term (see Supp. Matt. [29]),

$$\sum_i U_i \hat{n}_{\uparrow i}\hat{n}_{\downarrow i} \to \sum_i U_i \left(\hat{n}_{\uparrow i} - \frac{1}{2}\right)\left(\hat{n}_{\downarrow i} - \frac{1}{2}\right). \qquad (4)$$

For a spatially independent interaction, $U_i = U$, this change corresponds to a shift in the chemical potential, which leaves the non-equilibrium dynamics unaffected. This is however *not* the case for a spatially dependent interaction, where the additional symmetry dramatically affects the dynamics. Naively, by expanding the RHS of (4) we obtain an effective disordered potential, $\sum_i U_i \hat{n}_i/2$, which might lead one to suspect that the system is localized (note that the single-particle spectrum is still trivial). This reasoning is however misleading, since the potential and the disordered interaction are perfectly correlated and therefore a more detailed analysis is in order. If the hopping term is set to zero, the eigenstates of the system including the ground state are highly degenerate, since moving a doublon to an empty site does not cost energy. Therefore the doublons do not "feel" the presence of an effective disordered potential. In the limit of *zero* hopping the system is trivially localized; for small, but *non-zero* hopping, $\Delta U \gg t_h$, and for initial condition without singlons, the dynamics of the system

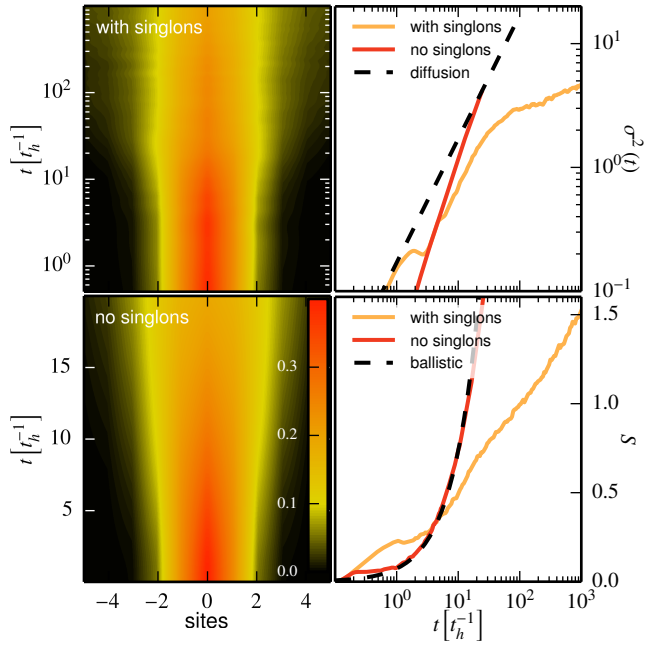

Figure 4. Same as Fig. 2 but with interaction term of Eq. (4). The data has been obtained using ED for $L = 11$ and $\Delta U = 30$, and averaged over at least 300 realizations. Note that the simulation time was $t = 1000$ for initial conditions with singlons, and $t = 100$ for the initial conditions without singlons.

is effectively described by the random Heisenberg model,

$$\hat{H}_{\text{eff}} = \sum_{ij} \frac{2t_h^2}{|U_{ij}|} \left(\hat{\mathbf{S}}_i \cdot \hat{\mathbf{S}}_j - \frac{1}{4} \right), \tag{5}$$

where the $\hat{\mathbf{S}}_i$ are spin-1/2 operators, $U_{ij} \equiv (U_i + U_j)/2$, and the derivation was performed along the lines of the derivation of the Heisenberg model from the Hubbard model [29, 34]. The random Heisenberg model was previously studied using strong disorder renormalization group. While the ground state is a localized random singlet state [37], at finite temperatures the renormalization group breaks down, which previously was interpreted as the onset of delocalization [38, 39]. Our results are consistent with this prediction. By projecting away all the singlons from the random initial configurations, we use ED to study transport [40]. We find (see Fig. 4) that entanglement entropy spreads ballistically, and charge excitations propagate super-diffusively. However, the super-diffusive propagation of the charge is likely a result of the relatively short times for which bulk transport is accessible in our simulations ($t \approx 25$), and the asymptotic charge transport is probably diffusive. Indeed for domain wall initial conditions we were able to observe diffusion even on this short timescale [29]. By performing a canonical transformation, $\hat{c}_{i\uparrow} \to \hat{c}^\dagger_{i\uparrow}$, $\hat{c}_{i\downarrow} \to (-1)^i \hat{c}^\dagger_{i\downarrow}$, the Hamiltonian maps to $-H$, namely, the many-body spectrum of this model is symmetric with respect to zero energy. Moreover, this transformation maps doublons and holons into singlons, which suggests that if doublons are delocalized (as we have shown), also singlons are delocalized for the transformed problem. Since the dynamics under $-H$ is equivalent to dynamics under H with a reversed direction of time, and since H is time-reversal invariant, we conclude that singlons are delocalized for H itself. Interestingly, starting with an initial condition which includes all possible charge configurations, namely a mix of doublons, holons and singlons, renders the charge transport *slower*. After a a relatively short diffusive regime, transport becomes sub-diffusive, or perhaps even logarithmic. Correspondingly, the entanglement entropy crosses-over from ballistic growth to a growth which is slightly faster than logarithmic (see Fig. 4). The mechanism behind the observed slow charge transport is currently not clear, and more detailed consideration of finite size effects in this regime is needed. It is however clear that the seemingly minor change in the form of the interaction (4) dramatically changes the system dynamics and leads to delocalization.

Experimental implementation.–The Fermi-Hubbard model has been extensively studied with ultracold atoms [41]. Tight-binding is achieved by loading the atoms to the lowest band of an optical lattice and the strength of interaction is controlled by tuning the s-wave scattering length using a magnetic Fano-Feshbach resonance. We suggest here to implement spatially random interactions between particles by means of optical Feshbach resonance with a random optical control. With the recent advances in quantum gas microscopy, this will allow the scattering strength to be controlled on a sub-micron spatial resolution. Optical Feshbach resonances are known to incur excess heating due to spontaneous emission from the excited state, and that could be detrimental for realizing many-body localization. To mitigate this effect, we suggest to use a scheme in which the light couples the bound Feshbach molecular state to an excited molecular state off-resonantly [42, 43]. Using this scheme the heating time can be as long as 10ms [44], which is about $50t_h^{-1}$ [9]. Since our numerical results show that localization occurs in less than $10t_h^{-1}$ we conclude that losses incurred by the optical control technique should not prevent one from observing and detecting the MBL phase.

Discussion.– We have established many-body localization in one-dimensional random Hubbard model with a completely delocalized single-particle spectrum which is *not* amenable to the theoretical analysis of Refs. [3, 27]. We proposed a realization of this model in cold atom experiments using spatially resolved optical Feshbach resonances [42, 43]. In this model, many-body localization follows from fragmentation of particles into slow and fast species (doublons and singlons), which is a result of the strong interactions. One species is Anderson localized by the quenched disordered potential and localizes the other

species by creating an effective chain of randomly distributed barriers. The mechanism for localization that we posit here is similar to recent proposals for MBL in clean systems, where two different species are introduced from the outset [13–16, 18, 20, 45], with the crucial difference that the effective disorder in our case is quenched, while it is annealed in the clean case. We believe that this is the main reason why, unlike here, the observation of MBL is challenging in the clean case [18], unless one of the species is completely immobile [45]. We demonstrated the importance of the initial conditions for observation of MBL in experimentally attainable timescales, and have shown that localization is absent when the model has *an additional* $SU(2)$ symmetry in the charge sector.

Note added.– During the completion of the manuscript three studies have appeared with relevance to the work presented here. Ref. [46] presents a numerical study of a distinct model with a completely delocalized single particle spectrum. In Ref. [47] a related *translationally invariant* model, which is also $SU(2)$ symmetric, was numerically studied. For sufficiently high interaction strength and generic initial conditions the authors show evidence of nonergodic behavior, consistent with our observations here. The work of Ref. [48] advocates for the impossibility of MBL in a system with non-Abelian continuous symmetry, which is *inconsistent* with our results. For this reason we present an extensive analysis of possible finite time and size effects in the Supplementary Materials [29]. It remains unclear if all arguments of Ref. [48] apply to our model. In particular, we work with initial charge configurations which *individually* dynamically break the $SU(2)$ symmetry, such that the symmetry is only satisfied after an average over *all* charge configuration is performed.

Acknowledgemnts.– YBL would like to thank Igor Aleiner for many enlightening and helpful discussions. DRR would like to thank Romain Vasseur for a useful correspondence. This work was supported by National Science Foundation Grant No. CHE-1464802. DMRG calculations were performed using the ITensor library, http://itensor.org.

* yb2296@columbia.edu

[1] P. W. Anderson, Phys. Rev. **109**, 1492 (1958).
[2] L. Fleishman, D. C. Licciardello, and P. W. Anderson, Phys. Rev. Lett. **40**, 1340 (1978).
[3] D. Basko, I. L. Aleiner, and B. L. Altshuler, Ann. Phys. (N. Y). **321**, 1126 (2006).
[4] E. Altman and R. Vosk, Annu. Rev. Condens. Matter Phys. **6**, 383 (2015).
[5] R. Nandkishore and D. A. Huse, Annu. Rev. Condens. Matter Phys. **6**, 15 (2015).
[6] R. Vasseur and J. E. Moore, (2016), arXiv:1603.06618.
[7] D. Basko, I. L. Aleiner, and B. L. Altshuler, Phys. Rev. B **76**, 052203 (2007).
[8] M. Ovadia, D. Kalok, I. Tamir, S. Mitra, B. Sacépé, and D. Shahar, Sci. Rep. **5**, 13503 (2015).
[9] M. Schreiber, S. S. Hodgman, P. Bordia, H. P. Luschen, M. H. Fischer, R. Vosk, E. Altman, U. Schneider, and I. Bloch, Science (80-.). **349**, 842 (2015).
[10] P. Bordia, H. P. Lüschen, S. S. Hodgman, M. Schreiber, I. Bloch, and U. Schneider, Phys. Rev. Lett. **116**, 140401 (2016).
[11] J. Smith, A. Lee, P. Richerme, B. Neyenhuis, P. W. Hess, P. Hauke, M. Heyl, D. a. Huse, and C. Monroe, (2015), arXiv:1508.07026.
[12] J.-y. Choi, S. Hild, J. Zeiher, P. Schauß, A. Rubio-Abadal, T. Yefsah, V. Khemani, D. A. Huse, I. Bloch, and C. Gross, (2016), arXiv:1604.04178.
[13] M. Schiulaz and M. Müller, in *AIP Conf. Proc.* (2014) pp. 11–23.
[14] T. Grover and M. P. A. Fisher, J. Stat. Mech. Theory Exp. **2014**, P10010 (2013).
[15] M. Schiulaz, A. Silva, and M. Müller, Phys. Rev. B **91**, 184202 (2015).
[16] N. Y. Yao, C. R. Laumann, J. I. Cirac, M. D. Lukin, and J. E. Moore, (2014), arXiv:1410.7407.
[17] J. M. Hickey, S. Genway, and J. P. Garrahan, (2014), arXiv:1405.5780.
[18] Z. Papić, E. M. Stoudenmire, and D. A. Abanin, Ann. Phys. (N. Y). **362**, 714 (2015).
[19] M. van Horssen, E. Levi, and J. P. Garrahan, Phys. Rev. B **92**, 100305 (2015).
[20] M. Pino, L. B. Ioffe, and B. L. Altshuler, Proc. Natl. Acad. Sci. **113**, 536 (2016).
[21] X. Li, S. Ganeshan, J. H. Pixley, and S. Das Sarma, Phys. Rev. Lett. **115**, 186601 (2015).
[22] X. Li, J. H. Pixley, D.-L. Deng, S. Ganeshan, and S. D. Sarma, (2016), arXiv:1602.01849.
[23] R. Modak and S. Mukerjee, (2016), arXiv:1602.02067.
[24] R. Modak and S. Mukerjee, Phys. Rev. Lett. **115**, 1 (2015).
[25] R. Vasseur, A. J. Friedman, S. A. Parameswaran, and A. C. Potter, Phys. Rev. B **93**, 134207 (2016).
[26] B. Bauer and C. Nayak, J. Stat. Mech. Theory Exp. **2013**, P09005 (2013).
[27] J. Z. Imbrie, J. Stat. Phys. **163**, 998 (2016).
[28] G. Vidal, Phys. Rev. Lett. **91**, 147902 (2003).
[29] "See supplemental material at [url] for a discussion of symmetries in the studied model, explanation of the chosen interaction strength, and additional discussion of finite size/time effects,".
[30] M. Žnidarič, T. Prosen, and P. Prelovšek, Phys. Rev. B **77**, 064426 (2008).
[31] J. H. Bardarson, F. Pollmann, and J. E. Moore, Phys. Rev. Lett. **109**, 017202 (2012).
[32] N. Strohmaier, D. Greif, R. Jördens, L. Tarruell, H. Moritz, T. Esslinger, R. Sensarma, D. Pekker, E. Altman, and E. Demler, Phys. Rev. Lett. **104**, 080401 (2010).
[33] R. Sensarma, D. Pekker, E. Altman, E. Demler, N. Strohmaier, D. Greif, R. Jördens, L. Tarruell, H. Moritz, and T. Esslinger, Phys. Rev. B **82**, 224302 (2010).
[34] K. A. Chao, J. Spałek, and A. M. Oleś, Phys. Rev. B **18**, 3453 (1978).
[35] M. Žnidarič, Phys. Rev. Lett. **106**, 220601 (2011).
[36] Due to the small size of our system, the obtained exponent is somehow larger that the exponent obtained in

Ref. [35], which is 4/3.
[37] S.-k. Ma, C. Dasgupta, and C.-k. Hu, Phys. Rev. Lett. **43**, 1434 (1979).
[38] K. Agarwal, E. Demler, and I. Martin, Phys. Rev. B **92**, 184203 (2015).
[39] R. Vasseur, A. C. Potter, and S. A. Parameswaran, Phys. Rev. Lett. **114**, 217201 (2015).
[40] Interestingly, the times for which bulk transport can be obtained in ED are very similar to the times accessible in tDMRG for same numerical cost. We therefore use ED for this part.
[41] T. Esslinger, Annu. Rev. Condens. Matter Phys. **1**, 129 (2010).
[42] D. M. Bauer, M. Lettner, C. Vo, G. Rempe, and S. Dürr, Phys. Rev. A **79**, 1 (2009).
[43] D. M. Bauer, M. Lettner, C. Vo, G. Rempe, and S. Dürr, Nat. Phys. **5**, 339 (2009).
[44] Z. Fu, P. Wang, L. Huang, Z. Meng, H. Hu, and J. Zhang, Phys. Rev. A **88**, 041601 (2013).
[45] A. E. Antipov, Y. Javanmard, P. Ribeiro, and S. Kirchner, (2016), arXiv:1605.01390.
[46] P. Sierant, D. Delande, and J. Zakrzewski, (2016), arXiv:1607.00227.
[47] J. R. Garrison, R. V. Mishmash, and M. P. A. Fisher, (2016), arXiv:1606.05650.
[48] A. C. Potter and R. Vasseur, (2016), arXiv:1605.03601.
[49] E. H. Lieb and D. W. Robinson, Commun. Math. Phys. **28**, 251 (1972).
[50] M. Friesdorf, A. H. Werner, W. Brown, V. B. Scholz, and J. Eisert, Phys. Rev. Lett. **114**, 170505 (2015).

I. SUPPLEMENTARY MATERIALS

Here we elaborate on the symmetries of the studied models, derive the effective Hamiltonian, as well as motivate the chosen disordered interaction strength.

A. Symmetries

Even with spatially dependent interactions the Hamiltonian,

$$\hat{H} = -t \sum_{i\sigma} \left(\hat{c}^{\dagger}_{i\sigma} \hat{c}_{i+1,\sigma} + \hat{c}^{\dagger}_{i+1,\sigma} \hat{c}_{i,\sigma} \right) + \sum_{i} U_i \hat{n}_{\uparrow i} \hat{n}_{\downarrow i}, \tag{S1}$$

has a $SU(2)$ symmetry with respect to the rotation of the spin, with the following generators,

$$\begin{aligned} \hat{S}^{z} &= \frac{1}{2} \sum_{i} \left(\hat{n}_{i\uparrow} - \hat{n}_{i\downarrow} \right) \\ \hat{S}^{+} &= \sum_{i} \hat{c}^{\dagger}_{i\uparrow} \hat{c}_{i\downarrow} \\ \hat{S}^{-} &= \sum_{i} \hat{c}^{\dagger}_{i\downarrow} \hat{c}_{i\uparrow}. \end{aligned} \tag{S2}$$

The modified Hamiltonian,

$$\begin{aligned} \hat{H}' = -t \sum_{i\sigma} \left(\hat{c}^{\dagger}_{i\sigma} \hat{c}_{i+1,\sigma} + \hat{c}^{\dagger}_{i+1,\sigma} \hat{c}_{i,\sigma} \right) + \\ + \sum_{i} U_i \left(\hat{n}_{\uparrow i} - \frac{1}{2} \right) \left(\hat{n}_{\downarrow i} - \frac{1}{2} \right), \end{aligned} \tag{S3}$$

has an additional $SU(2)$ symmetry in the charge sector, which follows particle-hole symmetry,

$$\hat{c}_{i\sigma} \rightarrow (-1)^{i} \hat{c}^{\dagger}_{i\sigma}. \tag{S4}$$

Its symmetry group is therefore $SU(2) \times SU(2)$. An additional symmetry which exists for the (S3) Hamiltonian in the $(N = L, S_z = 0)$ sector is that the eigenvalues satisfy, $E \longleftrightarrow -E$.

B. Selection of the disordered interaction strength

To delineate the phase diagram of the system we study the properties of its eigenstates using exact diagonalization. For this purpose we calculate the entanglement entropy of all the eigenstates. We first obtain the reduced density matrix,

$$\rho_A(E) = \mathrm{Tr}_{\bar{A}} \left| \psi(E) \right\rangle \left\langle \psi(E) \right|, \tag{S5}$$

for every eigenstate $|\psi(E)\rangle$, where A is a subsystem (we chose it to be the left half of the system) and $\bar{A}$ is its complimentary. The entanglement entropy is then defined as,

$$S(E) = -\mathrm{Tr}\ \rho_A(E) \log_2 \rho_A(E). \tag{S6}$$

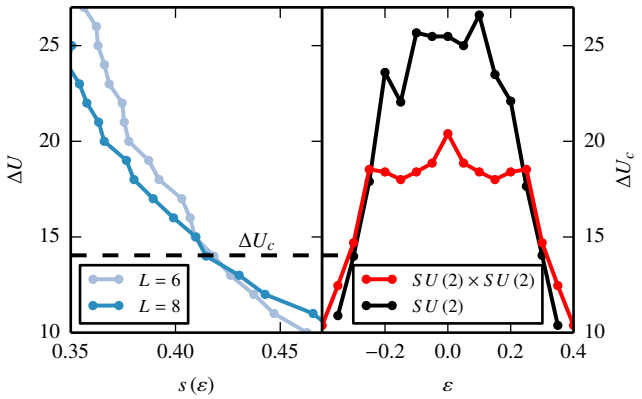

Figure S1. *Left panel*: entanglement entropy density ($s(\varepsilon)$) is plotted for various values of interaction disorder for a fixed energy density, $\varepsilon = -0.3$, and the $SU(2)$ symmetric version of model, (S1). *Right panel*: the critical interaction disorder (mobility edge) is plotted versus the energy density ε for both for models (S1) [black] and (S3) [red].

We will designate by $s(\varepsilon) = S(\varepsilon)/L$ the entanglement entropy density, and take $\epsilon \equiv (E - E_{\min})/(E_{\max} - E_{\min}) - 0.5$, to be the renormalized unitless energy density, which lies in the interval $\varepsilon \in [-0.5, 0.5]$. For one-dimensional systems which we consider in this work, $s(\varepsilon)$ is expected to be independent of system size if the system is ergodic, and to be inversely proportional to system size for a non-ergodic system. The location of the transition could be therefore obtained by the calculation of $s(\varepsilon)$ for various disorder strengths and energy densities. This procedure is presented in Fig. S1. On the left panel we obtain the location of the mobility edge ΔU_c, for a fixed energy density, ϵ. This is inferred from the intersection point of plots of $s(\varepsilon)$ for various system sizes. Each $s(\varepsilon)$ is obtained by calculating $S(\varepsilon)$ and averaging over a small interval of energy densities $\delta\varepsilon = 0.04$, as also 1000 disorder realization. In the left panel of Fig. S1 we demonstrate this procedure for the model (Eq. 1) for $\varepsilon = -0.3$. Due to the fast growth of the Hilbert space (4^L) we have access to only two system sizes, $L = 6$ and 8 in the sector $N = L$, $S_z = 0$. After repeating the outlined procedure for a number of energy densities we obtained the mobility edge, $\Delta U_c(\varepsilon)$, as a function of the energy density for both symmetric and non-symmetric versions of the model. As one can see from the right panel of Fig. S1, it has a typical domed shape with states in the middle of the band less localized than the states with lower (higher) energy densities.

Since in this work we are interested in demonstrating localization we choose $\Delta U = 30$, such that *all* many-state are expected to be localized for *both* versions of the model.

C. Derivation of the Effective Hamiltonian

We write the Hamiltonian as

$$\hat{H} = \hat{H}_K + \hat{H}_U, \tag{S7}$$

where $\hat{H}_U$ is the interaction term,

$$\hat{H}_U = \sum_i U_i \left(\hat{n}_{\uparrow i} - \frac{1}{2}\right)\left(\hat{n}_{\downarrow i} - \frac{1}{2}\right) \tag{S8}$$

and

$$\hat{H}_K \equiv \sum_{i\sigma} t_{ij}\hat{c}^\dagger_{i\sigma}\hat{c}_{j\sigma}, \tag{S9}$$

is the perturbation. For $U_i < 0$ the ground state of $\hat{H}_U$ contains only doublons and is 2^L times degenerate, since a doublon and a holon have same energies. We define a projector on the zero and doubly occupied states as, $\hat{P}$ and its complimentary as, $\hat{Q} = 1 - \hat{P}$. Then the Hamiltonian can be written in a block form,

$$\hat{H} = \hat{P}\hat{H}\hat{P} + \hat{Q}\hat{H}\hat{Q} + \left(\hat{P}\hat{H}\hat{Q} + \hat{Q}\hat{H}\hat{P}\right). \tag{S10}$$

We further divide the Hamiltonian into unperturbed, $\hat{H}_0 = \hat{P}\hat{H}\hat{P} + \hat{Q}\hat{H}\hat{Q}$ and perturbed parts, $\hat{H}_1 = \hat{P}\hat{H}\hat{Q} + \hat{Q}\hat{H}\hat{P}$, and note that $\left[\hat{P}, \hat{H}_0\right] = 0$ but $\left[\hat{P}, \hat{H}_1\right] \neq 0$. By performing a unitary transformation we eliminate the off-diagonal term up to second order in $\hat{H}_1$. Using Baker-Cambell-Hausdorff formula we can write,

$$\begin{aligned} e^S \hat{H} e^{-S} = \hat{H}_0 + \left[S, \hat{H}_0\right] + \frac{1}{2!}\left[S, \left[S, \hat{H}_0\right]\right] + \cdots \\ + \hat{H}_1 + \left[S, \hat{H}_1\right] + \frac{1}{2!}\left[S, \left[S, \hat{H}_1\right]\right] + \cdots. \end{aligned} \tag{S11}$$

Setting,

$$\left[S, \hat{H}_0\right] = -\hat{H}_1, \tag{S12}$$

we can recast the series into the form,

$$\begin{aligned} e^S \hat{H} e^{-S} = \hat{H}_0 + \left(\frac{1}{1!} - \frac{1}{2!}\right)\left[S, \hat{H}_1\right] \\ + \left(\frac{1}{2!} - \frac{1}{3!}\right)\left[S, \left[S, \hat{H}_1\right]\right] + \cdots. \end{aligned} \tag{S13}$$

The effective Hamiltonian to second order in the off-diagonal terms is therefore given by,

$$\hat{H}_{\text{eff}} = e^S \hat{H} e^{-S} = \hat{H}_0 + \frac{1}{2}\left[S, \hat{H}_1\right]. \tag{S14}$$

To calculate S we use (S12) in the unperturbed basis,

$$\left\langle \alpha \middle| \left[S, \hat{H}_0\right] \middle| \beta \right\rangle = S_{\alpha\beta}\left(E^{(0)}_\beta - E^{(0)}_\alpha\right) = -\left\langle \alpha \middle| \hat{H}_1 \middle| \beta \right\rangle, \tag{S15}$$

and therefore,

$$S_{\alpha\beta} = \frac{\left\langle \alpha \middle| \hat{P}\hat{H}\hat{Q} + \hat{Q}\hat{H}\hat{P} \middle| \beta \right\rangle}{E^{(0)}_\alpha - E^{(0)}_\beta}. \tag{S16}$$

In case that $\hat{P}$ projects to a degenerate subspace, such that $\hat{H}_0\hat{P}\left|\alpha\right\rangle = E^{(0)}_P\hat{P}\left|\alpha\right\rangle$, we can write,

$$\hat{S} = \hat{P}\hat{H}\left(E^{(0)}_P - \hat{H}_0\right)^{-1}\hat{Q} - \hat{Q}\left(E^{(0)}_P - \hat{H}_0\right)^{-1}\hat{H}\hat{P}. \tag{S17}$$

After some algebra we obtain the effective Hamiltonian,

$$\hat{H}_{\text{eff}} = E^{(0)}_P + \sum_{ijkl,\sigma\sigma'} \frac{t_{ij}t_{kl}}{U_{ij}}\hat{P}\hat{c}^\dagger_{k\sigma'}\hat{c}_{l\sigma'}\hat{c}^\dagger_{i\sigma}\hat{c}_{j\sigma}\hat{P}, \tag{S18}$$

where

$$U_{ij} \equiv \frac{U_i + U_j}{2}. \tag{S19}$$

Finally defining the following pseudo-spin operators,

$$\hat{S}^+_i = \hat{c}^\dagger_{i\uparrow}\hat{c}^\dagger_{i\downarrow} \qquad \hat{S}^-_i = \hat{c}_{i\downarrow}\hat{c}_{i\uparrow}, \qquad \hat{S}^z_i = \frac{1}{2}\left(\hat{n}_{i\downarrow} + \hat{n}_{i\uparrow} - 1\right), \tag{S20}$$

and using the properties of the projectors we obtain the anti-ferromagnetic random Heisenberg model,

$$\hat{H}_{\text{eff}} = E^{(0)}_P + \sum_{ij} \frac{2\left|t_{ij}\right|^2}{\left|U_{ij}\right|}\left(\hat{\mathbf{S}}_i \cdot \hat{\mathbf{S}}_j - \frac{1}{4}\right). \tag{S21}$$

D. Finite time and finite size effects

As in any numerical study, our results are limited to finite sizes and times. It is therefore pertinent to present evidence that the observed behavior persists also for larger systems and longer times. We would like to consider three possible objections to the observed localization, all related to the relatively high U we use in our simulation:

1. For small systems and large interaction, $U/t_h \gg 1$, the many-body spectrum includes gaps, which effectively makes the system non-ergodic [S18].

2. The system size is too small to either break apart the localized doublons, or to build a large, almost "classical" quasi-particle along the scenario of delocalization introduced in Ref. [S48].

3. The time it takes to observe delocalization is beyond the reach of our simulations.

We argue that the existence of gaps in the many-body spectrum does not *necessarily* imply localization, moreover some of the gaps may very well persist in the thermodynamic limit [S47]. In Fig. S2 we present the many-body eigenvalues of models (S1) and (S3) for a single

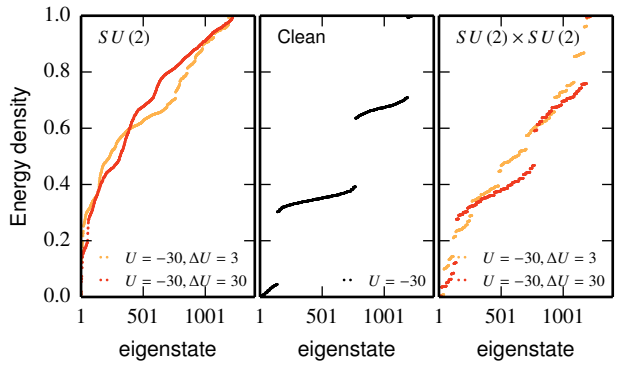

Figure S2. Eigenvalues of a single disorder realization normalized to lie in the interval $[0, 1]$. *Left panel*: $SU(2)$ symmetric model, (S1), for $\Delta U = 3$ (light orange) and $\Delta U = 30$ (dark orange). *Central panel*: clean system, $\Delta U = 0$. *Right panel*: same as left panel but for the $SU(2) \times SU(2)$ symmetric model (S3). For all models $L = 7$.

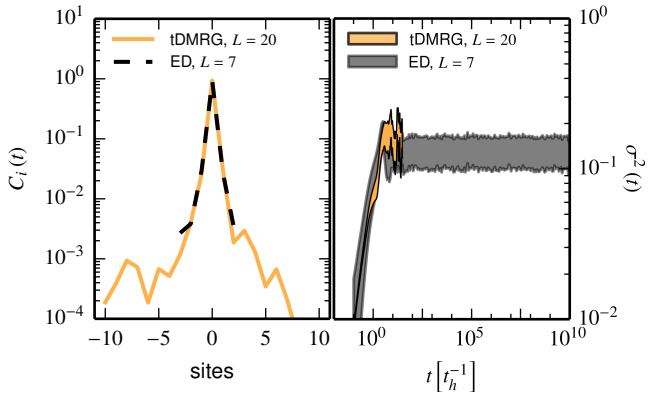

Figure S3. Charge excitation dynamics for starting from a random charge configuration *without* singlons calculated using tDMRG simulation for $L = 20$ (orange) and ED for $L = 7$ (black/gray). *Left panel*: Excitation profile at the final times of the simulation $L = 7$, $t = 10^{10}$ and $L = 20$, $t = 30$. *Right panel*: charge excitation width as a function of time on a log-log plot. Shades designate uncertainty due to averaging. The parameters used are $-30 \leq U_i \leq 0$.

disorder realization, as well as the eigenvalues of the corresponding clean model $(\Delta U = 0)$. Gaps exist for all three models. In fact, since for the disordered models we use $-\Delta U \leq U_i \leq 0$, gaps are *smaller* for larger ΔU, since disorder enlarges the phase space of possible $(U_1 + U_2 + \cdots)$ combinations. Therefore the largest gaps appear for $\Delta U = 0$, when only multiples of U are possible. The transport, on the other hand, is very different in all three models. It varies from localized, delocalized to subdiffusive, as we present in the main text. This shows that having gaps in the many-body spectrum need not have direct implications for ergodicity.

The second point concerns the finite size of the system. For small systems, some excitations might never decay. For example, due to energy conservation, a doublon with an energy of U would *never* decay in a system of N particles, if the maximal change of the single particles is $\delta_{\max}$, such that $U > \delta_{max} N$. For larger systems a collective (though very rare) excitation of the particles would be able to break the doublon apart. However since this process requires a delicate cooperation of the particles the decay rate of the doublon would be exponentially slow [S33]. Since in the model we study (1) a finite doublon density is necessary to localize the singlons, one may question: **a)** if localization might be lost due to doublon decay **b)** the small system size prevents the decay to occur. We argue that a *finite* doublon density will never decay to zero for sufficiently strong interaction even for *infinite* systems. This means that the mechanism of localization due to doublons may exist also in the thermodynamic limit, though with (slightly) renormalized disorder strength. To show that finite doublon density cannot decay, we repeat the above argument for a finite system with a minor modification. By duplicating the small system, and using energy conservation, it is easy to see that the maximal change in the doublon density is $\delta n_d = O(1/U)$, which means that for sufficiently large U a *finite* density of doublons cannot decay completely even in an *infinite* system. Moreover a finite doublon density implies that the temperature is $T \approx U$, for which the processes required for the decay of the doublons are not rare anymore, and occur at the rate of t_h. The change of the effective disordered potential as a result of the doublon decay is about $O(1/U)$. We thus claim that the effect of the decay of the doublon density on localization is negligible for large U.

In Ref. [S48] it is suggested that for $SU(2)$ symmetric models the local degrees of freedom will join into large "quasi-classical" objects which will induce delocalization. One might therefore suspect that either the system is too small to create such a large object, or alternatively the creation and motion of such objects might occur at later times. This study however does not specify what are the required length and time scales to observe delocalization in such models.

In our work we calculate the spread of a *local* excitation which is described by the correlation function,

$$C_i(t) = \frac{1}{\mathrm{Tr}\ \hat{P}} \mathrm{Tr}\ \hat{P} \left(\hat{n}_i(t) - 1\right)\left(\hat{n}_0 - 1\right). \tag{S22}$$

The locality of the operators which appear in the correlation function, as well as the locality of the Hamiltonian (1), guarantee

$$\left\| \left\langle \hat{O}_i(t)\, \hat{O}_j \right\rangle \right\| \leq \exp\left[-a\left(|i-j| - vt\right)\right], \tag{S23}$$

following from rigorous Lieb-Robinson bounds [S49],

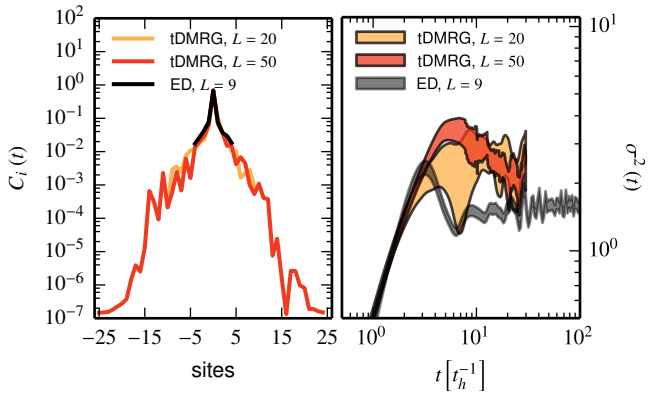

Figure S4. Charge excitation dynamics for starting from a random charge configuration *(no constraints)* calculated using tDMRG simulation for $L = 20$ and 50 (light and dark orange) and ED for $L = 9$ (black/gray). *Left panel*: Excitation profile at the final times of the simulation $L = 9$, $t = 100$ and $L = 20, 50$, $t = 30$. *Right panel*: charge excitation width as a function of time on a log-log plot. Shades designate uncertainty due to averaging. The parameters used are $-30 \leq U_i \leq 0$.

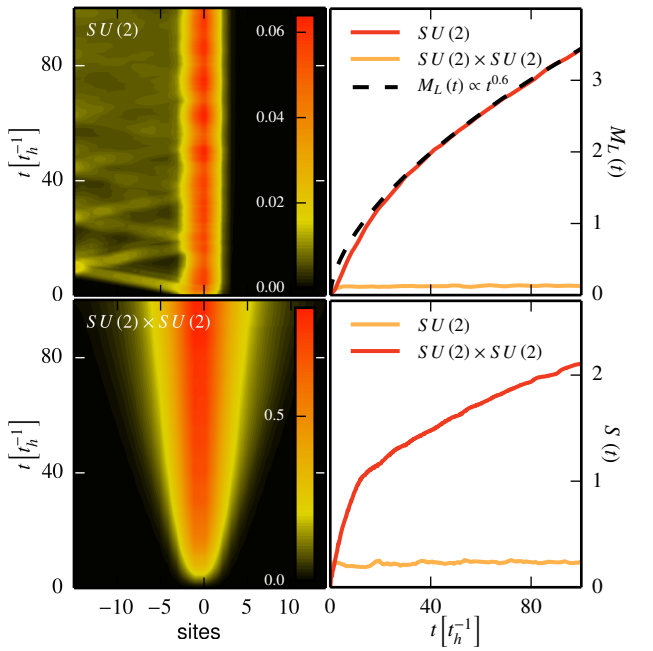

Figure S5. On the left, the charge density perturbation, $\langle \hat{n}_i(t) - \hat{n}_i(0) \rangle$, is plotted vs time and space for models (S1) [top] and (S3) [bottom]. On the right the total charge on the LHS, $M_L(t)$, is plotted versus time on the top panel and the entanglement entropy, $S(t)$ versus time is plotted on the bottom. The data has been obtained using tDMRG for $L = 30$ and $\Delta U = 30$, and averaged over at least 300 disorder realizations.

where v is the maximal spread velocity, which is of order of the hopping rate (here $O(1)$). This means that for any *finite* time, the excitation is bounded by an exponential in the distance $|i - j|$, namely it is effectively contained in a finite box. *Finite size* effects could be therefore eliminated to any required precision *up to any finite time*. For localized systems the bound is uniform in time, which signifies the absence of transport [S50]. In our work, by looking at the profile of the excitation as well as its width, we show that for the $SU(2)$ symmetric model (S1) this bound is indeed uniform at least up to some finite time. As can be seen from the left panel of Fig. S3, starting from an initial configuration of only doublons, the $L = 7$ system and the $L = 20$ system essentially give the same results, while compared at strikingly different times $t = 30$ ($L = 20$) versus $t = 10^{10}$ ($L = 7$). This signifies both absence of charge transport, and effective elimination of finite size effects. For *unconstrained* random initial configuration, as can be seen from Fig. S4, non-negligible residual tails of the excitation prevent elimination of finite size effects for a system size of $L = 9$ (ED). Nevertheless, the excitation profile stays almost the same across increasing system sizes of $L = 9$, 20 and 50, and the width of the excitation appears to be converged already for $L = 20$. The tDMRG simulation demands considerable resources in this regime due to the initial fast growth of the entanglement entropy, which results from ballistic motion of the singlons between the doublons. This results in poor averaging (100-300 realizations) and a bias towards more localized charge configurations. Notwithstanding, the appearance of localization plateau, while less convincing compared to "doublons only" case, is evident here as well.

E. Domain wall initial condition

We have also considered the dynamics starting from a domain wall initial conditions. This type of initial conditions is more amenable to experimental study in cold atoms [S12]. We have chosen an initial condition such that the right half of the system is completely full, while the left half is empty, and measured the total number of particles on the LHS, $M_L(t)$. In Fig. S5 one can see the profile on the charge density perturbation, $\langle \hat{n}_i(t) - \hat{n}_i(0) \rangle$, on the left, as also the charge transfer, $M_L(t)$ and $S(t)$ on the right. For the $SU(2)$ symmetric model described by (S1) the ballistic jet of the singlons is clearly visible, as is its reflections from the simulation boundaries as well. The core of the system however remains localized. The $SU(2) \times SU(2)$ symmetric model described by (S3) is clearly delocalized and on the accessible time scales exhibits transport very close to diffusive,

$$M_L(t) \propto t^{0.6}, \tag{S24}$$

with entanglement entropy which is almost linearly growing with time.